PCCP

Accepted Manuscript

ROYAL SOCIETY OF CHEMISTRY

www.rsc.org/pccp

PCCP

ARTICLE

Staircase patterns of nuclear fluxes during coherent tunneling in excited doublets of symmetric double well potentials

Received 00th January 20xx,
Accepted 00th January 20xx

DOI: 10.1039/x0xx00000x

www.rsc.org/

ChunMei Liu,[a,b] Jörn Manz[a,b,c] and Yonggang Yang[a,c]

Tunneling isomerizations of molecules with symmetric double well potentials are associated with periodic nuclear fluxes, from the reactant R to the product P and back to R. Halfway between R and P the fluxes achieve their maximum values at the potential barrier. For molecules in the lowest tunneling doublet (v=0) the rises and falls to and from the maximum values are approximately bell-shaped. Upon excitations to higher tunneling doublets v=1,2, etc, however, this shape is replaced by symmetric "staircase patterns" of the fluxes, with v+1 steps up and down in the domains of R and P, respectively. The quantum derivation of the phenomenon is universal. It is demonstrated here for a simple model of nuclear fluxes during tunneling isomerization of ammonia along the umbrella inversion mode, with application to separation of isotopomers.

Introduction

The quantum theory of concerted electronic and nuclear fluxes (CENFs) in molecules that react from reactants (R) to products (P) by coherent tunneling in symmetric double well potentials has been presented recently, as part of the Perspective.[1] The results therein are for tunneling in the lowest tunneling doublet (labeled by quantum number v=0) that is supported by the double well potential. Extensions to nuclear fluxes during coherent tunneling in asymmetric double well potentials have also been published recently, again for the lowest tunneling doublet, v=0.[2]

The purpose of this paper is to extend the previous investigation[1] to coherent tunneling in excited tunneling doublets, v=1,2,....This extension is motivated by various discoveries for tunneling in the doublet v=0, which serves as a reference. For example, all CENFs by tunneling in v=0 flow synchronously.[1] The derivation in Ref. 1 is valid for arbitrary molecular processes which involve two eigenstates, hence the synchronicity of the CENFs holds not only for tunneling in the ground state doublet v=0, but also in excited doublets v=1,2,.... Focusing on nuclear fluxes during tunneling in doublet v=0, it has been shown that these fluxes can be written as products of spatial times temporal factors[1-5]. The temporal factor accounts for periodic tunneling from R to P and back to R, during the tunneling time τ that is related to the tunneling splitting Δe by Hund's famous equation $\tau \cdot \Delta e = h.$ [6] Hund's derivation[6] implies that this relation holds for all tunneling doublets v=0,1,2,...

$$\Delta e_v \cdot \tau_v = h. \quad (1)$$

The spatial factors of the nuclear fluxes during tunneling in doublet v=0 are symmetric, with bell-shaped rises and falls in the domains of R and P, from zero via maximum values back to zero.[1-5] The maxima are half way between R and P, at the potential barrier between R and P. On first glance, this result appeared paradoxical because the nuclear density is always localized at either R or P, but never at the potential barrier. How can the flux then have its maximum at the barrier? This result was rationalized by saying that the systems do not like to tunnel, instead they prefer to stay in configurations R or P. But since quantum mechanics dictates that they must tunnel from R to P and back to R,[6] they make it through the barrier as fast as possible, hence the fluxes achieve their maximum values at the barrier.[5] Quite unexpectedly, it was discovered that the bell-shaped symmetry of the nuclear fluxes holds not only during tunneling in symmetric double well potentials, but also in asymmetric ones.[2] All these phenomena associated with nuclear fluxes in the ground-state doublet (v=0), which are rather surprising, motivated the present search for additional effects engendered by tunneling in excited doublets (v= 1,2,...) of molecules with symmetric double well potentials. A key question is whether the symmetric spatial bell-type shapes of the fluxes for v=0 persist for tunneling in excited doublets v=1,2,... Different shapes, e.g. quantum carpet type[7] or quantum accordion type[8] patterns have already been discovered for nuclear fluxes at even higher energies, beyond tunneling.

The results will be demonstrated for a simple example. The new phenomenon is universal, however, i.e. it holds for all molecules with symmetric double well potentials. At the end of this paper, we also propose an experiment for separation of isotopomers by tunneling in different levels v=0 and v>0.

[a] State Key Laboratory of Quantum Optics and Quantum Optics Devices, Institute of Laser Spectroscopy, Shanxi University, 92 Wucheng Road, Taiyuan 030006, China.
[b] Institut für Chemie und Biochemie, Freie Universität Berlin, Takustrasse 3, 14195 Berlin, Germany.
[c] Collaborative Innovation Center of Extreme Optics, Shanxi University, 92 Wucheng Road, Taiyuan 030006, China.

In view of the Perspective[1], this paper should make a new contribution to the emerging field of research on intramolecular fluxes, including nuclear[2-12], electronic[13-29] as well as CENFs.[1,30-43] The general importance of intramolecular fluxes in reaction dynamics and the microscopic foundation of chemical kinetics is documented in the monography (44).

Model, theory and methods

As model system for demonstrations of nuclear fluxes during tunneling in excited doublets *v*=1,2,... of double well potentials, and for comparisons with the phenomena in the ground state doublet *v*=0, we adapt the one-dimensional (1D) model of tunneling isomerization of ammonia by umbrella inversion from Ref. (45), see also Ref. (46). The model assumes conservation of C_{3v} symmetry, fixed NH bond lengths, fixed molecular orientation, and fixed nuclear center of mass. In the NCM frame, the protons move along equivalent arcs about the nucleus of the nitrogen atom. These arcs define the nuclear coordinate *q* for umbrella inversion. The corresponding symmetric 1D double-well potential $V(q)=V(-q)$ is adapted from Ref. (45). It is shown in Figures 1, 2, 3 below; it has also been used in Refs. (2,4,5). Its barrier height, $V_b = V(q=0) = 2022.18\ hc\cdot\mathrm{cm}^{-1}$, is attained at the planar configuration, $q = 0$ Å. The "left" and "right" potential minima, $V(q_R)=V(q_P)=0\ hc\cdot\mathrm{cm}^{-1}$ at $\pm q_R = \mp q_P = \pm 0.3925$ Å, specify the classical configurations of the "reactant" (R) and "product" (P). For convenience the associated domains of the "left" (*q*<0) and "right" (*q*>0) potential wells are defined as R and P, respectively. The model uses isotopomer (subscript "*i*") selective reduced masses μ_i [45]. It is validated by excellent agreement of the calculated and experimental mean energies $\overline{e}_{iv}$ and tunneling splittings Δe_{iv} for all levels *v* below V_b and for all isotopomers $^{14}NH_3$, $^{15}NH_3$, $^{14}ND_3$, $^{15}ND_3$, $^{14}NT_3$, as documented in Table 1[45-55]. Here these isotopomers are labeled *i*=1,2,...,5, respectively. Table 1 also lists the tunneling times $\tau_{iv} = h/\Delta e_{iv}$ (see eqn. (1)), and results predicted for $^{15}NT_3$ (*i*=6). Evidently the tunneling times decrease with decreasing mass M_i and corresponding reduced mass μ_i of the isotopomer, and also with excitation to higher levels *v* of the tunneling doublets.

The tunneling doublets of isotopomers *i* with levels *v* = 0, 1, 2, ... are characterized by their mean energies $\overline{e}_{iv} = (e_{iv+} + e_{iv-})/2$ and their tunneling splittings $\Delta e_{iv} = e_{iv-} - e_{iv+}$. These are defined in terms of the eigen-energies e_{iv+} and e_{iv-} with parities + and -. The eigen-energies are determined, together with the corresponding orthonormal sets of eigenfunctions $\phi_{iv+}(q)$ and $\phi_{iv-}(q)$, by diagonalizing the 1D model Hamiltonian $H = -\frac{\hbar^2}{2\mu_i}\frac{\partial^2}{\partial q^2} + V(q)$ by means of the fast Fourier Transform (FFT) discrete-variable representation (DVR). The corresponding normalized wavefunctions and nuclear probability densities (NPDs) representing R and P of isotopomers *i* in levels *v* are $\psi_{iv,R} = (\phi_{iv+} + \phi_{iv-})/\sqrt{2}$, $\rho_{iv,R} = |\psi_{iv,R}|^2$ and $\psi_{iv,P} = (-\phi_{iv+} + \phi_{iv-})/\sqrt{2}$, $\rho_{iv,P} = |\psi_{iv,P}|^2$, respectively.[1,2] The NPDs of R and P are mirror images of each other,

$$\rho_{iv,R}(q) = \rho_{iv,P}(-q)\ . \qquad (2)$$

The nodal structures of the eigenfunctions imply simple lobe-structures of the NPDs of R and P. Specifically, $\rho_{iv,R}(q)$ and $\rho_{iv,P}(q)$ consist of *v* bell-shaped lobes in the domains of R and P, respectively. The lobes are well separated from each other. The relation (2) implies that these lobes are also mirror images of each other in the domains of R and P. In contrast, the NPDs of R and P are entirely negligible in the complementary domains of P and R, respectively.

Starting from R in level *v*, the NPD of isotopomer *i* evolves as[1,2]

$$\rho_{iv,R}(q,t) = \rho_{iv,R}(q) + \left[\rho_{iv,P}(q) - \rho_{iv,R}(q)\right]\sin^2(\pi t/\tau)\ . \qquad (3)$$

Accordingly it oscillates periodically as the system tunnels from R at *t* = 0, τ_{iv} , $2\tau_{iv}$, ... etc to P at $t = \tau_{iv}/2$, $3\tau_{iv}/2$, $5\tau_{iv}/2$, and back to R. The resulting nuclear flux density (NFD) or flux is[1,2]

$$j_{iv,R}(q,t) = \int_{q_0}^{q}\left[\rho_{iv,R}(q') - \rho_{iv,P}(q')\right]dq' \cdot (\pi/\tau_{iv})\sin(2\pi t/\tau_{iv}) \qquad (4)$$

Apparently, the nuclear flux depends on the level *v* of isotopomer *i*. Eqn. (4) also confirms that the nuclear fluxes are products of spatial times temporal factors. The temporal factor is sinusoidal with amplitude π/τ_{iv} and period τ_{iv} , corresponding to alternating positive and negative flux during tunneling from R to P and back to R during time intervals (0, $\tau_{iv}/2$), (τ_{iv} , $3\tau_{iv}/2$), ... etc., and ($\tau_{iv}/2$, τ_{iv}), ($3\tau_{iv}/2$, $2\tau_{iv}$), ... etc., respectively. The spatial factor is an integral of the difference $\rho_{iv,R}(q) - \rho_{iv,P}(q)$ of the densities of R and P. The lower integration limit $q_0 = -1.0$ Å is chosen such that the integrand is negligible for $q < q_0$. The relation (2) implies that the differences of the NPDs are antisymmetric,

$$\rho_{iv,R}(q) - \rho_{iv,P}(q) = -\left[\rho_{iv,R}(-q) - \rho_{iv,P}(-q)\right]\ . \qquad (5)$$

Furthermore, the dominant contributions to the differences of the NPDs in the domains of R and P are $\rho_{iv,R}(q)$ and $\rho_{iv,P}(q)$, respectively. Their lobe-structures are, therefore, also antisymmetric, in accord with eqn (5). The antisymmetry (5) yields the symmetry of the NFDs,

$$j_{iv,R}(q,t) = j_{iv,R}(-q,t)\ . \qquad (6)$$

Hence, the rises of the spatial factors of the fluxes (4) in the domain of R (from 0 at q_0 to maximum values at *q*=0) are mirror images of their falls in the domain of P. The normalizations of the NPDs ($\int_{-\infty}^{+\infty}\rho_{iv,R}(q)dq = 1$ and $\int_{-\infty}^{+\infty}\rho_{iv,P}(q)dq = 1$) imply that the maximum values of the spatial profiles are close to 1. As a consequence, all the fluxes reach their maximum values ($\approx \pi/\tau_{iv}$) at the potential barrier (*q*=0), halfway between R and P (at $t = \tau_{iv}/4$).

Results and discussions

We are now ready for the key point of this paper. It is based on expression (4) for the NFDs, on the antisymmetry (5), and on the lobe-structure of the difference of the NPDs (see the discussions after eqns. (2) and (5)). The differences of the NPDs of R and P are illustrated in Figures 1a, 2a, 3a, exemplarily for levels *v*=0, 1, 2 of isotopomers *i*=1 ($^{14}NH_3$), 1 and 5 ($^{14}NT_3$), respectively. The spatial integral (4) in the domain of R encompasses the successive lobes of $\rho_{iv,R}(q)$ starting from the lobe nearest to q_0. Each of these positive lobes thus adds a "step" to the value of the flux. The NPD of an isotopomer in level *v* has *v*+1 lobes that generate, therefore, the nuclear tunneling flux with *v*+1 "steps up" in the domain of R. Likewise, $-\rho_{iv,P}(q)$ in the domain of P has *v*+1 negative lobes which appear as the inverse of the positive lobes in the domain of R. Integration of these lobes yields the flux in the domain of P with

corresponding *v*+1 "steps down". Altogether the spatial profile of the nuclear flux appears as a symmetric staircase with *v*+1 steps up and down in the domains of R and P, respectively. This is illustrated in Figures 1b, 2b, 3b, for the cases of *v*+1=1, 2, 3 "steps up and down" for isotopomers *i*=1,1,5 in levels *v*=0, 1, 2, respectively. For example, Figure 2a shows the difference of the NPDs of $^{14}NH_3$(*v*=1) with two positive lobes in the domain of R which are separated from each other at $q_{R1} = -0.369$ Å. Accordingly, the nuclear flux shown in Figure 2b has two steps up in the domain of R, also separated at $q_{R1} = -0.369$ Å. Likewise, the difference of the NPDs has corresponding two negative lobes in the domain of P, causing two steps down in the nuclear flux, separated at $q_{P1} = 0.369$ Å. Figures 3a and 3b for $^{14}NT_3$ show analogous separations of three positive plus three negative lobes of the difference of the NPDs in the domains of R and P, causing three steps up and down in the nuclear fluxes, separated at $q_{R1} = -0.430$ Å, $q_{R2} = -0.296$ Å and at $q_{P1} = 0.430$ Å, $q_{P2} = 0.296$ Å, respectively. In retrospect, the example of $^{14}NH_3$(*v*=0) shown in Figures 1a and 1b (adapted from Ref. (2)) appear as special case with single positive and negative lobes of the difference of the NPDs in the domains of R and P, corresponding to one-step rises and falls of the nuclear densities in the domains of R and P, respectively. Finally, the corresponding NPDs (3) and NFDs (4) are illustrated by contour diagrams in Figures 1c, 2c, 3c and 1d, 2d, 3d, respectively. The results for isotopomers $^{15}NH_3$ (*i*=2) and $^{15}NT_3$ (*i*=6) in levels 0, 1 and 2 are similar to those of $^{14}NH_3$ (*i*=1) and $^{14}NT_3$ (*i*=5); in fact they are almost indistinguishable on the scale of Figures 1, 2, 3.

Conclusions and outlook

The present "staircase patterns" of nuclear fluxes are complementary to patterns of "quantum carpets" and the "quantum accordion" which have been reported in Refs. (7) and (8), respectively. They may be monitored experimentally, e.g., by means of pump-probe spectroscopy, see Ref. (8). It is easy to predict analogous staircase patterns of nuclear fluxes in systems with cyclic symmetric double-well potentials (e.g. in molecules with torsional degrees of freedom.[4,5]) The cyclic boundary condition opens two equivalent clockwise and anticlockwise paths for tunneling from one potential minimum representing R to the opposite one representing P. Symmetry breaking by external electric fields may support one of the paths while suppressing the other.[2] As a consequence, clockwise tunneling from R to P will alternate with anti-clockwise tunneling from P to R, which is reminiscent of alternating clockwise-anticlockwise electron circulations.[56,57] Again, the nuclear tunneling fluxes in excited states will exhibit staircase patterns.

Finally, as an outlook, we propose an experiment that makes use of tunneling in ground state and excited state doublets, for separations of isotopomers. The concept is adapted from Quack's approach to the even more demanding task, distinction of left- and right-handed enantiomers embedded in corresponding double well potentials, by means of the parity-violating energy difference ΔE_{PV} due to weak currents.[58-61] Quack's strategy consists of several steps, here we focus on the following. (For consistency of the notation in this paper, we allow the possibility of various molecular isotopomers *i*.) Consider first the scenario without weak currents. In order to be distinguishable, the different enantiomers must be separated by a very high potential barrier. As a consequence, the splittings Δe_{iv} of the lowest doublets are extremely narrow[6]. Now let us turn on the "perturbation" ΔE_{PV} of the weak current. There are two limiting cases which are labeled by (7b), (7c), and by analogy (9b), (9c) below. If the ratio

$$r_{iv,PV} = \Delta e_{iv} / \Delta E_{PV} \qquad (7a)$$

is much larger than 1,

$$r_{iv,PV} >> 1 , \qquad (7b)$$

then the perturbation ΔE_{PV} is negligible and the system is dominated by the properties of the double-well potential, thus supporting delocalized eigenstates as described above. On the other hand, if

$$r_{iv,PV} << 1 , \qquad (7c)$$

then the "perturbation" ΔE_{PV} is dominant. Consequently the molecular eigenstates are localized, representing either left- or right-handed enantiomers. Quack considers the scenario (7c). His trick for measuring ΔE_{PV} is to prepare the system in a parity-selective state in an excited doublet. Since this state is *not* an eigenstate of the system, it evolves from one parity to the other with period

$$\tau_{PV} = h / \Delta E_{PV} , \qquad (8)$$

analogous to eqn. (1).[58-61]

We propose an analogous trick for separating the least abundant isotopomer $^{15}NT_3$ (*i*=6) from all others (*i*=1,2,...,5). Instead of perturbations of the molecular double-well potentials by weak currents, we introduce perturbations by a *z*-polarized external electric field $E = E_m + z \cdot \frac{dE}{dz}$ with mean value E_m and inhomogeneity $\frac{dE}{dz}$. For simplicity, we assume that the ammonia molecules have been oriented along *z* (e.g., by the methods of Refs. (62-65)). Accordingly the ratio (7a) is replaced by

$$r_{iv,E_m} = \Delta e_{iv} \Big/ \left| -\langle \phi_{iv+} | d \cdot E_m | \phi_{iv-} \rangle \right| \qquad (9a)$$

where $-\langle \phi_{iv+} | d \cdot E_m | \phi_{iv-} \rangle$ is the interaction of the electric field E_m with the transition dipole (*d*) of isotopomer *i* at doublet *v*. As for the limits (7b), (7c), the cases

$$r_{iv,E_m} >> 1 \qquad (9b)$$

and

$$r_{iv,E_m} << 1 \qquad (9c)$$

yield delocalized and localized eigenstates, respectively. Reactant states, which are constructed as superpositions of the delocalized states tend to tunnel periodically, as described above. Hence the long time averages of the dipoles (called "mean dipoles" below) approach the zero limit, $\langle d_{iv} \rangle \to 0$. In contrast, case (9c) blocks tunneling, that means the reactants remain trapped in the reactant well of the double-well potential, and the mean dipoles approach the rather large values of the reactants, $\langle d_{iv} \rangle \to \langle d_{iv} \rangle_R$.[2]

For any given isotopomer *i* in level *v* with tunneling splitting Δe_{iv} one can choose sufficiently weak or strong electric fields E_m in order to achieve the limits (9b) or (9c), respectively. Specifically, for an electric field of about 80kV/m,

isotopomers *i*=1,2,3,4 in level *v*=0 (the dominant level at low temperature) as well as *i*=5 excited to *v*=1 approach the limit (9b), whereas the target isomer $^{15}NT_3$ (*i*=6) approaches the limit (9c). As a consequence, the mean dipole $\langle d_{i=6,v=0} \rangle$ of isotopomer *i*=6 in level *v*=0 is rather large compared with all others. Hence, one can employ the inhomogeneous field component $z \cdot \frac{dE}{dz}$ in order to drive the target isotopomer *i*=6 away from all others. The success of this separation of isotopomers rests on the excitation of isotopomer 5 to level *v*=1, causing tunneling by two-step fluxes with corresponding low values of the mean dipole. After the separation of the isotopomer *i*=6, one can use the same concept to separate the other isotopomers sequentially with suitable electric fields and inductions of fluxes with staircase patterns in the first or higher excited states.

Acknowledgements

One of us (J.M.) thanks Prof. M. Quack (ETH Zürich) for stimulating discussions of his method and guidance to the literature (58-61). We are also grateful to Prof. D. J. Diestler (Lincoln) for careful reading and polishing the manuscript. Generous financial support by the Deutsche Forschungsgemeinschaft DFG (project Ma 515/27-1), the 973 Program of China (Grant No.2012CB921603), the talent program of Shanxi, the Natural Science Foundation of Shanxi, China (2014021004), the National Natural Science Foundation of China (NSFC, Grant nos. 11434007, 61378015), and the Program for Changjiang Scholars and Innovative Research Team (IRT13076) are also gratefully acknowledged.

Notes and references

1 T. Bredtmann, D. J. Diestler, S.-D. Li, J. Manz, J. F. Pérez-Torres, W.-J. Tian, Y.-B. Wu, Y. Yang and H.-J. Zhai, *Phys. Chem. Chem. Phys.,* 2015, **17**, 29421.
2 C. Liu, J. Manz, Y. Yang, *J. Phys. B: At. Mol. Opt. Phys,* 2015, **48**, 164001.
3 T. Bredtmann, H. Kono, J. Manz, K. Nakamura, C. Stemmle, *ChemPhysChem,* 2013, **14**, 1397.
4 T. Grohmann, J. Manz, A. Schild, *Mol. Phys.* 2013, **111**, 2251.
5 J. Manz, A. Schild, B. Schmidt, Y. Yang, *Chem. Phys.,* 2014, **442**, 9.
6 F. Hund, *Z. Phys.*, 1927, **43**, 805.
7 T. Bredtmann, H. Katsuki, J. Manz, K. Ohmori, C. Stemmle, , *Mol. Phys.*, 2013, **111**, 1691.
8 J. Manz, J. F. Pérez-Torres, Y. Yang, *Phys. Rev. Lett.*, 2013, **111**, 153004.
9 A. Accardi, I. Barth, O. Kühn, J. Manz, *J. Phys. Chem. A*, 2010, **114**, 11252.
10 I. Barth, C. Bressler, S. Koseki, J. Manz, *Chem. Asian J.* 2012, **7**, 1261.
11 J. F. Pérez-Torres, *Phys. Rev. A*, 2015, **91**, 022510.
12 I. Barth, C. Daniel, E. Gindensperger, J. Manz, J. F. Pérez-Torres, A. Schild, C. Stemmle, D. Sulzer, Y.Yang, in "*Advances in Multi-PhotonProcesses and Spectroscopy"* 2015, **22**, 59-110. eds. S.H. Lin, A. A. Villaeys, Y. Fujimura, (World Scientific, Singapore).
13 I. Barth, J. Manz, *Angew. Chem. Int. Ed.*, 2006, **45**, 2962.
14 I. Barth, J. Manz, Y. Shigeta, K. Yagi, *J. Am. Chem. Soc.*, 2006, **128**, 7043.
15 I. Barth, J. Manz, in "*Progress in Ultrafast Intense Laser Science VI, Springer Series in Chemical Physics",* 2010, ***99***, 21-44, eds. K. Yamanouchi, A. D. Bandrauk, G. Gerber (Springer, Berlin, 2010)
16 H.-C. Hege, J. Manz, F. Marquardt, B. Paulus, A. Schild, *Chem. Phys.*, 2010, **376**, 46.
17 T. Bredtmann, J. Manz, *Angew. Chem. Int. Ed.*, 2011, **50**, 12652.
18 J. Manz, K. Yamamoto, *Mol. Phys.*, 2012, **110**,517.
19 T. Bredtmann, E. Hupf, B. Paulus, *Phys. Chem. Chem. Phys.*, 2012, **14**, 15494.
20 M. Okuyama, K. Takatsuka, *Chem. Phys. Letters*, 2009, **476**, 109.
21 T. Yonehara, K. Takatsuka, *Chem. Phys.*, 2009, **366**, 115.
22 K. Nagashima, K. Takatsuka, *J. Phys. Chem. A*, 2009, **113**, 15240.
23 K. Takatsuka, T. Yonehara, *Adv. Chem. Phys.*, 2009, **144**, 93.
24 K. Takatsuka, T. Yonehara, *Phys. Chem. Chem. Phys.*2011, **13**, 4987.
25 M. Okuyama, K. Takatsuka, *Bull. Chem. Soc. Jpn.*, 2012, **85**, 217.
26 K. Nagashima, K. Takatsuka, *J. Phys. Chem. A*, 2012, **116**, 11167.
27 K. Takatsuka, T. Yonehara, K. Hanasaki, Y. Arasaki, *Chemical Theory Beyond the Born-Oppenheimer Paradigm: Nonadiabatic Electronic and Nuclear Dynamics in Chemical Reactions* (World Scientific, New Jersey, 2015).
28 P. von den Hoff, I. Znakovskaya, S. Zherebtsov, M. F. Kling, R. de Vivie-Riedle, *Appl. Phys. B*, 2010, **98**, 659.
29 S. Patchkovskii, *J. Chem. Phys.*, 2012, **137**, 084109.
30 I. Barth, H.-C. Hege, H. Ikeda, A. Kenfack, M. Koppitz, J. Manz, F. Marquardt, G. K. Paramonov, *Chem. Phys. Lett.*, 2009, **481**, 118.
31 A. Kenfack, F. Marquardt, G. K. Paramonov, I. Barth, C. Lasser, B. Paulus, *Phys. Rev. A*, 2010, **81**, 052502.
32 A. Kenfack, I. Barth, F. Marquardt, B. Paulus, *Phys. Rev. A*, 2010, **82**, 062502.
33 D. Andrae, I. Barth, T. Bredtmann, H.-C. Hege, J. Manz, F. Marquardt, B. Paulus, *J. Phys. Chem. B*, 2011, **115**, 5476.
34 A. Kenfack, S. Banerjee, B. Paulus, *Phys. Rev. A*, 2012, **85**, 032501.
35 D. J. Diestler, *J. Phys. Chem. A*, 2012, **116**, 2728.
36 D. J. Diestler, A. Kenfack, J. Manz, B. Paulus, *J. Phys. Chem. A*, 2012, **116**, 2736.
37 D. J. Diestler, *J. Phys. Chem. A*, 2012, **116**, 11161.
38 D. J. Diestler, *J. Phys. Chem. A*, 2013, **117**, 4698.
39 J. F. Pérez-Torres, *Phys. Rev. A*, 2013, **87**, 062512.
40 D. J. Diestler, A. Kenfack, J. Manz, B. Paulus, J. F. Pérez-Torres, V. Pohl, *J. Phys. Chem. A*, 2013, **117**, 8519.
41 J. Manz, J. F. Pérez-Torres, Y. Yang, *J. Phys. Chem. A*, 2014, **118**, 8411.
42 J. F. Pérez-Torres, *J. Phys. Chem. A*, 2015, **119**, 2895.
43 G. Hermann, B. Paulus, J. F. Pérez-Torres, V. Pohl, *Phys. Rev. A*, 2014, **89**, 052504.
44 N. E. Henriksen and F. Y. Hansen, *Theories of Molecular Reaction Dynamics: The Microscopic Foundation of Chemical Kinetics*, Oxford University Press, New York, 2008.
45 J. R. Letelier, C. A. Utreras-Díaz, *Spectrochimica Acta Part A*, 1997, **53**, 247.
46 T. Rajamäki, M. Kállay, J. Noga, P. Valiron, L. Halonen, *Mol. Phys.* 2004, **102**, 2297.
47 V. Špirko, *J. Mol. Spectrosc.* 1983, **101**, 30.
48 W. Gordy. R. L. Cook, *Microwave Molecular Spectra, Intersciencs*, New York, 1970.
49 Š. Urban, V. Špirko, D. Papoušek, J. Kauppinen, S. P. Belov, L. I. Gershtein, A. F. Krupnov, *J. Mol. Spectrosc.*, 1981, **88**, 274.

50 Š. Urban, V. Špirko, D. Papoušek, R. S. McDowell, N. G. Nereson, S. P. Belov, L. I. Gershstein, A. V. Maslovskij, A. F. Krupnov, J. Curtis, K. N. Rao, *J. Mol. Spectrosc*., 1980, **79**, 455.
51 V. M. Devi, P. P. Das, K. N. Rao, Š. Urban, D. Papoušek, V. Špirko, *J. Mol. Spectrosc*., 1981, **88**, 293.
52 W. S. Benedict, E. K. Plyler, *Can. J. Phys.*, 1957, **35**, 1235.
53 P. Helminger, F. C. DeLucia, W. Gordy, H. W. Morgan, P. A. Staats, *Phys. Rev. A*, 1974, **9**, 12.
54 K. N. Rao, W. W. Brim, J. M. Hoffman, L. H. Jones, R. S. McDowell, *J. Mol. Spectrosc*., 1963, **7**, 362.
55 H. Jones, *J. Mol. Spectrosc.*, 1978, **70**, 279.
56 M. Kanno, H. Kono, Y. Fujimura, *Angew. Chem. Int. Ed.*, 2006, **45**, 7995.
57 M. Kanno, H. Kono, Y. Fujimura, S.H. Lin, *Phys. Rev. Lett.,* 2010, **104**, 108302.
58 M. Quack, *Chem. Phys. Lett.,* 1986, **132**, 147.
59 M. Quack, in: "*Femtosecond Chemistry*", 1995, **2**, 781-818. eds. J. Manz, L. Wöste, (Wiley VCH, Weinheim)
60 M. Quack, in: "*Handbook of High-Resolution-Spectroscopy*", 2011, **1**, 659-722. eds. M. Quack, F. Merkt, (John Wiley& Sons, Chichester)
61 M. Quack, *Eur. Rev.*, 2014, **22**, S50.
62 H. Stapelfeldt, T. Seideman, *Rev. Mod. Phys.*, 2003, **75**, 543.
63 F. Filsinger, J. Küpper, G. Meijer, L. Holmegaard, J. H. Nielsen, I. Nevo, J. L. Hansen, H. Stapelfeldt, *J. Chem. Phys.*, 2009, **131**, 064309.
64 S. Fleischer, Y. Zhou, R. W. Field, K. A. Nelson, *Phys. Rev. Lett.*, 2011, **107**, 163603.
65 G. Karras, E. Hertz, F. Billard, B. Lavorel, J.-M. Hartmann, O. Faucher, E. Gershnabel, Y. Prior, I. Sh. Averbukh, *Phys. Rev. Lett.*, 2015, **114**, 153601.

PCCP

ARTICLE

Table 1. Calculated mean energies $\bar{e}_{iv}$ above the ground state e_{i0+}, tunneling splittings Δe_{iv} and tunneling periods τ_{iv} of v=0,1,2… doublets for six isotopomers (i) of ammonia. Experimental data and previous theoretical results are given for comparison when available. All energies are in units of hc•cm^{-1}, times are in units of ps.

Isotopomer	i	ν	Mean energies $\bar{e}_{iv}$					
			This work	Experiment	Experiment[50]	Theory[47]	Theory[45]	Theory[46]
$^{14}NH_3$	1	0	0.403	0.395[48]	0.330	0.470	0.403	0.397
		1	950.282	950.265[49]	950.160	949.585	950.289	949.79
$^{15}NH_3$	2	0	0.384	0.380[54]		0.450	0.384	
		1	946.239	945.670[55]		945.240	946.402	
$^{14}ND_3$	3	0	0.0197	0.0250[51]		0.030	0.0195	
		1	746.749	747.375[51]		747.215	746.731	
		2	1398.335	1394.000[52]		1394.600	1398.304	
$^{15}ND_3$	4	0	0.0178	0.0250[51]		0.030	0.0180	
		1	741.293	741.005[51]		741.445	741.245	
		2	1389.585			1385.020	1389.505	
$^{14}NT_3$	5	0	0.00284	0.005[53]		0.025	0.003	
		1	654.032	656.780[54]		654.945	653.781	
		2	1245.410			1243.300	1244.986	
$^{15}NT_3$	6	0	0.00245					
		1	647.813					
		2	1234.785					

Table 1 (Continued):

Isotopomer	i	ν	Tuneling splittings Δe_{iv}						τ_{iv}
			This work	Experiment	Experiment[50]	Theory[47]	Theory[45]	Theory[46]	
$^{14}NH_3$	1	0	0.805	0.79[48]	0.66	0.94	0.805	0.793	41.4
		1	35.751	35.67[49]	35.84	38.41	35.757	35.62	0.93
$^{15}NH_3$	2	0	0.767	0.76[54]		0.90	0.768		43.5
		1	34.386	34.53[55]		37.1	34.442		0.97
$^{14}ND_3$	3	0	0.0394	0.05 [51]		0.06	0.039		845.3
		1	2.746	3.55 [51]		3.91	2.746		12.2
		2	59.618	70[52]		73.86	59.611		0.56
$^{15}ND_3$	4	0	0.0356	0.05[51]		0.06	0.036		935.8
		1	2.509	2.95[51]		3.59	2.508		13.3
		2	55.834			69.6	55.807		0.60
$^{14}NT_3$	5	0	0.00568	0.01[53]		0.05	0.006		5845.0
		1	0.483	0.82[54]		0.89	0.48		69.1
		2	15.178			23.38	15.113		2.2
$^{15}NT_3$	6	0	0.00490						6788.9
		1	0.422						79.1
		2	13.555						2.5

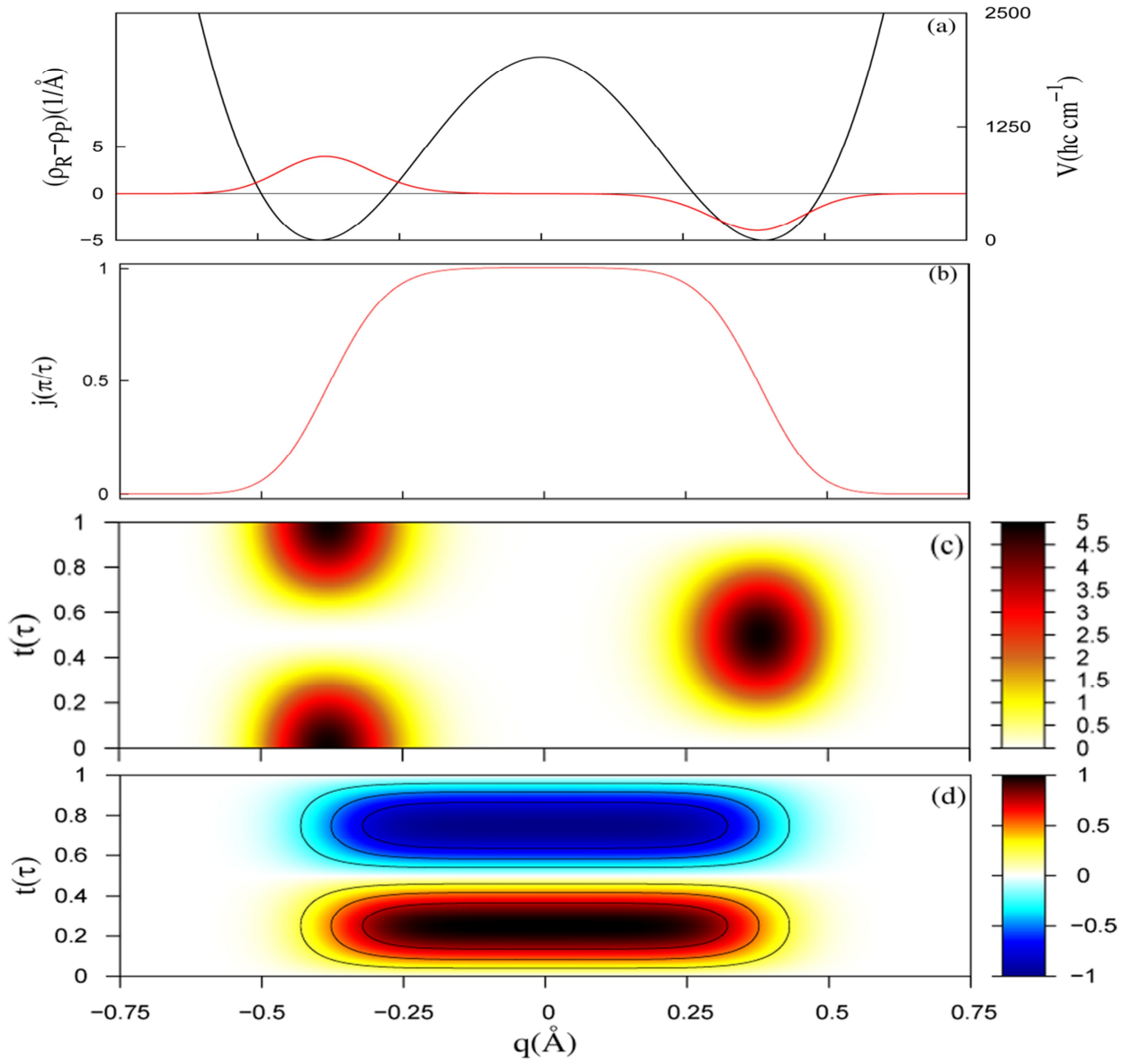

Figure 1. Nuclear probability density (NPD) and nuclear flux density (NFD) for the tunneling inversion of $^{14}NH_3$ at doublet *v*=0. (a): 1D potential energy curve V(*q*) (black) along the tunneling inversion coordinate *q* and the difference of the NPDs of the reactant R and product P (red). (b): NFD $j(q)$ at the time $t=\tau/4$ in units of π/τ, where $\tau=41.4\text{ps}$ for *v*=0. Panels (c) and (d) show the time evolutions of the NPD $\rho(q,t)$ (eqn. (3)) (c) and NFD $j(q,t)$ (eqn. (4)) (d), respectively.

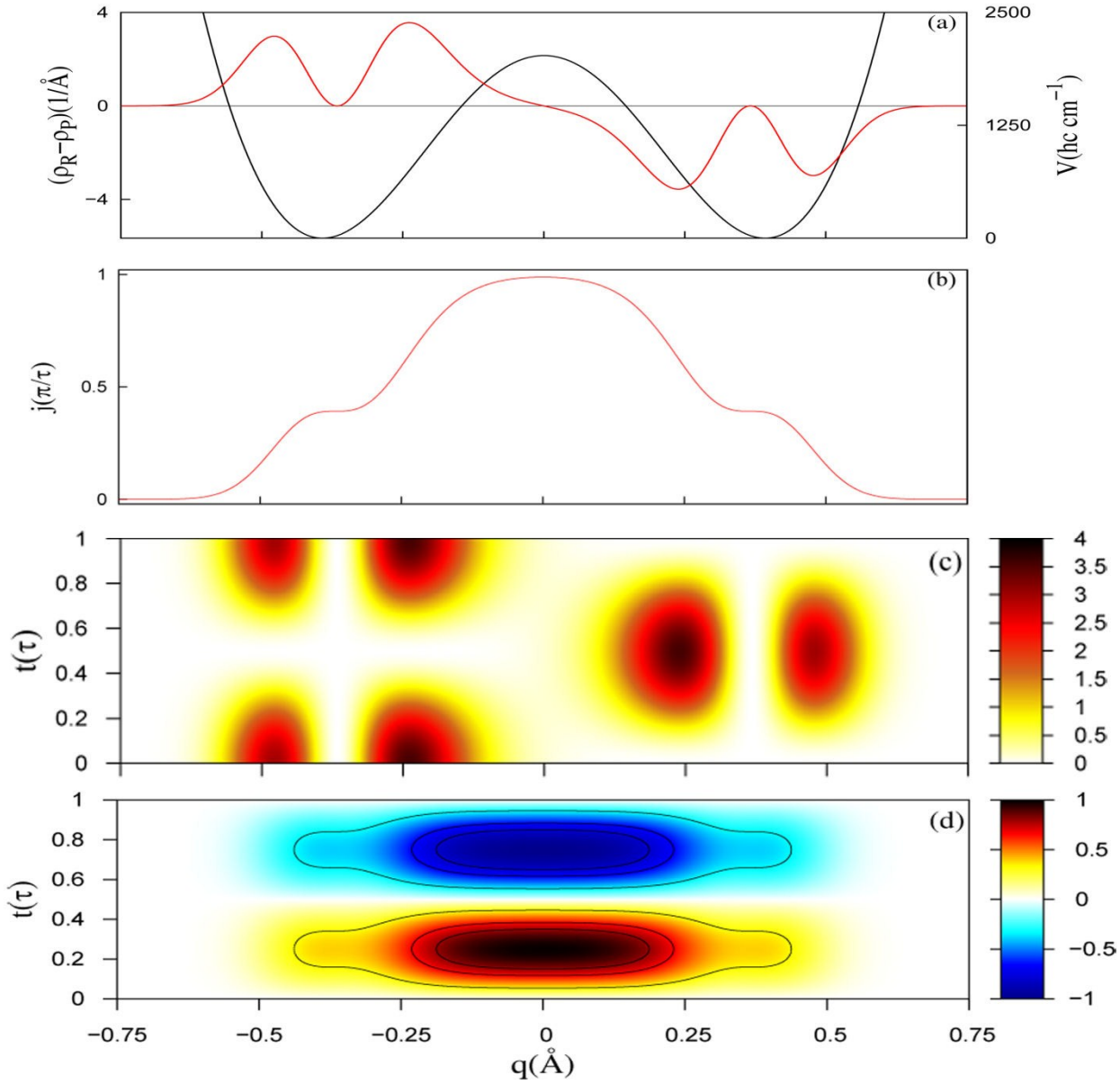

Figure 2. Nuclear probability density (NPD) and nuclear flux density (NFD) with staircase pattern for the tunneling inversion of $^{14}NH_3$ at doublet *v*=1. The tunneling period is $\tau = 0.93\text{ps}$. The notation is as in Fig. 1.

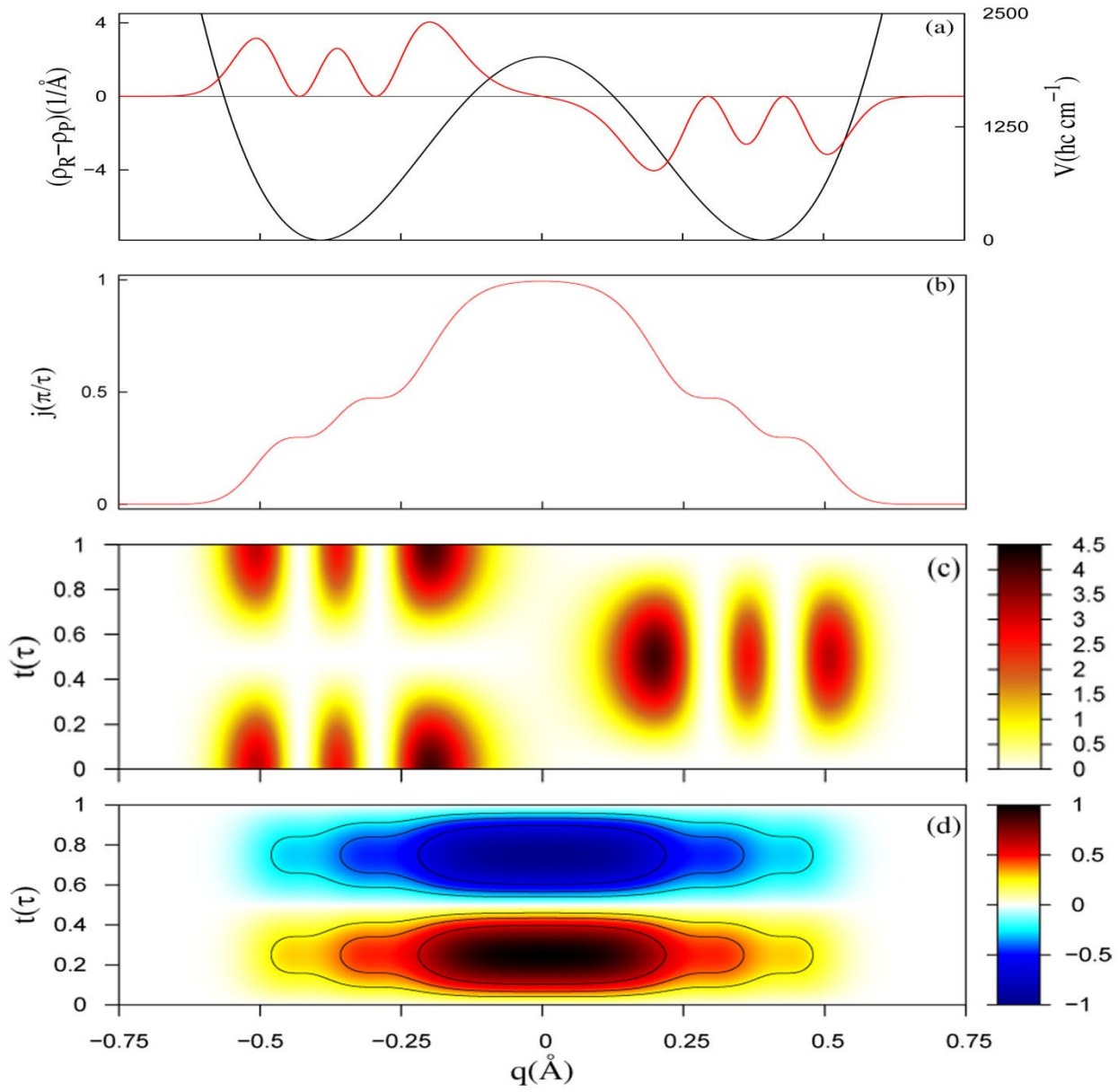

Figure 3. Nuclear probability density (NPD) and nuclear flux density (NFD) with staircase pattern for the tunneling inversion of $^{14}NT_3$ at doublet *v*=2. The tunneling period is $\tau = 2.2\text{ps}$. The notation is as in Fig. 1.